Available online at www.sciencedirect.com
SCIENCE DIRECT
Thermochimica Acta 440 (2006) 146–155
thermochimica acta
www.elsevier.com/locate/tca

Solid state thermochemical decomposition of neat 1,3,5,5-tetranitrohexahydropyrimidine (DNNC) and its DNNC-d_6 perdeuterio-labeled analogue

Scott A. Hendrickson [a,1], Scott A. Shackelford [b,*,2,3]

[a] *Department of Chemistry, Pt. Loma Nazarene University, San Diego, CA 92106-2899, USA*
[b] *Air Force Research Laboratory, Propellants Branch (AFRL/PRSP), 10 East Saturn Drive, Edwards AFB, CA 93524-7680, USA*

Received 6 September 2005; received in revised form 14 October 2005; accepted 6 November 2005
Available online 5 December 2005

Dedicated to the memory of Raymond N. Rogers (Los Alamos National Laboratory), a pioneer in isothermal DSC kinetic analysis, an outstanding scientist, a research mentor, collaborator, and true friend (dec. March 8, 2005)—SAS.

Abstract

The solid state thermochemical decomposition kinetics and activation energy of neat 1,3,5,5-tetranitrohexahydropyrimidine (DNNC) and its DNNC-d_6 deuterium labeled analogue were obtained by isothermal differential scanning calorimetry (IDSC) at 142, 145, and 148 °C. Global rate constants and kinetic deuterium isotope effect (KDIE) data from the exothermic decomposition process suggest that homolytic C–H bond rupture, in one or both types of chemically non-equivalent methylene (–CH_2) groups of the DNNC ring structure, constitutes the exothermic rate-controlling step. A DNNC-d_6 energy of activation equal to 115 kJ/mol was determined for this initial autocatalytic exothermic energy release from which a 106 kJ/mol activation energy was calculated for unlabeled DNNC. This exothermic autocatalytic decomposition process follows an extended endothermic induction period for DNNC which shows a higher 128 kJ/mol activation energy during which a catalytic initiating species may form by a rate-controlling step different from C–H bond rupture.
© 2005 Elsevier B.V. All rights reserved.

Keywords: 1,3,5,5-Tetranitrohexahydropyrimidine; DNNC; Solid state decomposition; Deuterium isotope effect; KDIE

1. Introduction

Global, heterogeneous reaction kinetics obtained via isothermal differential scanning calorimeter (IDSC) analyses often are ignored in favor of highly defined homogeneous kinetic studies that measure specific reaction steps. However, the global kinetics obtained from liquid and solid state thermochemical decomposition processes with neat high-energy compounds provide important data for practical technology and safety considerations [1]. An isothermal DSC analysis aptly demonstrated this point when the resultant global kinetics data from the solid state decomposition of 1,3,5-triamino-2,4,6-trinitrobenzene (TATB) was used to predict the critical temperature needed to initiate a thermal explosion event [2]. The critical temperature of an energetic compound defines the lowest constant surface temperature at which a compound, given a specific size, shape, and composition, can self-heat to a catastrophic event. When the global kinetic rate constant for this solid state TATB decomposition process was substituted into the Frank-Kamenetskii equation, the predicted 354 °C critical temperature matched its experimentally determined value [2].

Factors influencing global solid heterogeneous kinetic rates are decidedly different from those encountered in less complex homogeneous kinetic studies. Global reaction kinetics in condensed phase thermochemical decomposition heavily involve complex bimolecular reaction processes [3], and in the

* Corresponding author. Tel.: +1 661 275 5847; fax: +1 661 275 5471.
E-mail address: scott.shackelford@edwards.af.mil (S.A. Shackelford).
[1] Present address: Donald Bren School of Information and Computer Sciences, University of California, Irvine, CA 92697, USA.
[2] Experimental IDSC thermochemical decomposition investigations were conducted at The F.J. Seiler Research Laboratory, USAF Academy, CO, USA, prior to its September 30, 1995 decommissioning.
[3] Adjunct Professor, Pt. Loma Nazarene University, San Diego, CA, August 1997 to August 2003.

0040-6031/$ – see front matter © 2005 Elsevier B.V. All rights reserved.
doi:10.1016/j.tca.2005.11.007

solid state, describe reactions occurring within a thin zone of reactant–product contact that advance into the non-decomposed interior of the particle [1]. Other factors uniquely influencing global heterogeneous solid compound kinetic measurements include melting, impurities, and crystal defects [1]. For these reasons, when conducting kinetic deuterium isotope effect-based (KDIE) thermochemical decomposition analyses like those described in this investigation, it is important, whenever possible, to synthesize and prepare non-labeled and analogous deuterium-labeled compounds in an identical manner. This action ensures any kinetic rate differences found result solely from the deuterium atom substitution [4].

Given the importance of global heterogeneous kinetic and mechanistic data with energetic compounds, the solid state thermochemical decomposition process of 1,3,5,5-tetranitrohexahydropyrimidine (DNNC) and its DNNC-d_6 deuterium labeled analogue were investigated by isothermal DSC analysis using the kinetic deuterium isotope effect (KDIE) approach. A maximum sensitivity setting was used for the DSC instrument in order to detect minute curve deflections over short time intervals. The global reaction rate constants, resultant energies of activation, and the rate-controlling bond ruptures regulating the energy release rate for the neat solid state DNNC thermochemical decomposition process were determined.

DNNC is comprised of a unique heterocyclic hybrid chemical structure that incorporates features found in both high-energy geminal dinitroalkane and cyclic nitramine compounds (Fig. 1). The DNNC molecule contains two types of methylene groups [$-CH_2-$] sandwiched between two different energetic structural sites. One non-equivalent $-CH_2-$ group is sandwiched between two nitrated N atoms [$N-NO_2$] at the ring 1- and 3-positions, and two chemically equivalent $-CH_2-$ groups each flank the geminal dinitro-substituted ring carbon atom [$C(NO_2)_2$] at the 5-position. First synthesized in 1982 [5,6] the DNNC [7] hybrid structure is a high-energy pseudo-nitramine with an impact sensitivity significantly lower than that exhibited by the structurally related cyclic RDX nitramine. The explosive initiation sensitivity of DNNC resembles that of the more stable nitroaromatic TNT molecule, but when initiated, its detonation energy is significantly higher than TNT and rivals the RDX nitramine [5]. Thus, the DNNC pseudo nitramine exhibits energy and sensitivity properties associated with both nitramine and nitroaromatic compounds.

DNNC thermochemical stability also is similar to TNT in that it melts without noticeable or significant decomposition. A standard scanning DSC study used to determine the heat of fusion at its 154.8–156.2 °C melting point revealed no significant DNNC sample decomposition. Permitting the melted DNNC sample to re-solidify, then conducting an IDSC liquid thermochemical decomposition run at 176 °C gave virtually the same thermogram and heat of decomposition energy output as did a fresh DNNC sample at the same temperature [8]. Conversely, the symmetrical, cyclic six-membered RDX nitramine and its eight-membered HMX homologue undergo thermochemical decomposition during melting or liquefaction so rapidly that their heat of fusion cannot be determined [8].

Two thermal decomposition studies have been reported for DNNC. One decomposition was conducted in solvent (THF) at 105 °C at high-pressure (1.1 GPa) conditions. Under diluted solvent conditions, an apparent unimolecular process was inferred that produced a facile elimination of HNO_2 with no rate-controlling step reported [9]. Thermochemical decomposition processes conducted in solvents are quite different from the ambient pressure, neat solid state DNNC thermochemical decomposition conditions of this investigation where bimolecular processes likely predominate.

A second thermochemical decomposition investigation with neat DNNC and several of its 5-substituted (Fig. 1) derivatives employed T-Jump/FTIR and Raman spectroscopy analyses at 0.5 MPa and 350 °C. Results suggested that the substituted groups at the 5-position largely control the pathway followed by the predominantly bimolecular decomposition process and determine the gaseous products observed [10]. Once again, no rate-controlling step was identified. While structural features at the 5-position may determine a specific pathway for the thermochemical decomposition process, homolytic bond rupture kinetically controls the rate at which this DNNC decomposition pathway proceeds. The rate-controlling bond rupture, and the activation energy required to initiate it, recently were presented for the both the DNNC solid and liquid state decomposition processes in an abbreviated format [11].

Identification of this rate-controlling chemical bond rupture during the ambient pressure thermochemical decomposition process is a key mechanistic feature of energetic compound behavior. The same rate-controlling bond rupture seen in the thermochemical decomposition process for both nitroaromatic and nitramine compounds mirrors that found in the more drastic high-pressure and -temperature combustion and explosion events [12]. Indeed, it also appears that this rate-controlling chemical bond rupture is a key mechanistic

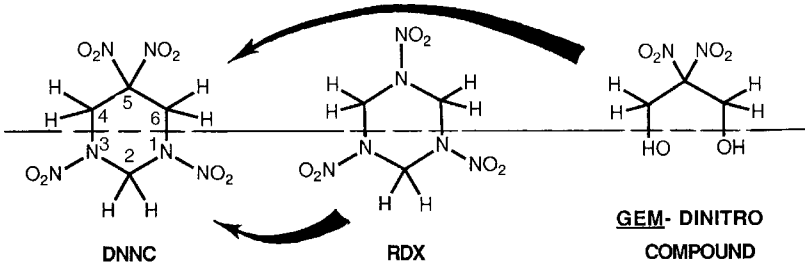

Fig. 1. Intramolecular hybrid structure of the DNNC molecule.

step in energetic compound global initiation and sensitivity properties [13].

Amid the myriad of complex simultaneous and sequential chemical reactions that proceed during the thermochemical decomposition process, the kinetic deuterium isotope effect (KDIE) approach, used with ambient pressure IDSC analysis, has identified this critical rate-controlling bond rupture, first with liquid TNT (2,4,6-trinitrotoluene) [17], and subsequently, for solid TATB (1,3,5-triamino-2,4,6-trinitrobenzene) [2], liquid and solid HMX (octahydro-1,3,5,7-tetranitro-1,3,5,7-tetrazocine), [16] liquid RDX (1,3,5-trinitrohexahydro-1,3,5-triazine),[18] and their respective deuterium-labeled TNT-α-d_3, TATB-d_6, HMX-d_8, RDX-d_6 analogues. The rate-controlling step also has been determined using isothermal thermal gravimetric analyses (TGA) with HMX/HMX-d_8 and RDX/RDX-d_6 nitramines, since they produce mainly gaseous products during their liquid and solid state thermochemical decomposition processes [19]. While the rate-controlling bond rupture may or may not constitute the first homolytic bond rupture during a complex thermochemical decomposition process, this bond rupture occurs during the slowest step of a coherent, steady-state reaction. This key reaction and its rate-controlling bond rupture predominate over all other reactions during a specific portion of the complex decomposition process, and thereby, kinetically regulate the overall rate at which the process proceeds.

In every case, the same rate-controlling bond rupture found in the ambient pressure thermochemical decomposition process for a given energetic compound [2,12,16–19] also appears to be the rate-controlling step for high-pressure combustion [4,12,20] and the predominant rate-controlling feature in explosive initiation events [2,12,19,21–26].

Using the maximum IDSC instrument sensitivity settings, this report investigates the ambient pressure solid state thermochemical decomposition mechanism of neat DNNC between 142 and 148 °C, below its melting point range of 154.8–156.2 °C [8]. Following a 3–5 h endothermic induction period, DNNC undergoes a very slow but significant exothermic thermochemical decomposition process. IDSC analyses conducted with DNNC and DNNC-d_6, coupled with the kinetic deuterium isotope effect (KDIE) approach, identify the rate-controlling bond rupture that governs the rate at which the solid state decomposition proceeds and permits its energy of activation to be determined.

2. Experimental

2.1. Instrumental and chemical details

The IDSC thermochemical decomposition curves were obtained using a Perkin-Elmer DSC 7 instrument set to its maximum sensitivity. Perkin-Elmer stainless steel large volume capsules (LVC), part no. 0319–1526 (top) and 0319–1525 (bottom) were used without Viton O-ring seals, part no. 0319–1535. DNNC and DNNC-d_6 sample sizes ranging from 1.50 to 1.54 mg were weighed into the LVC capsules and then sealed in the open atmosphere. During the IDSC thermochemical decomposition, the sealed capsules were under a stream of nitrogen gas using the highest instrumental sensitivity setting immediately following a contractor-accomplished instrumental calibration and fine tuning service call. To ensure utmost accuracy, the DSC 7 temperature was calibrated with indium (m.p. 156.60 °C) prior to each IDSC sample run. A total of 32 IDSC runs were conducted. Six runs were conducted on DNNC at 148 and 145 °C, while five runs were conducted each on DNNC at 142 °C and DNNC-d_6 at 148, 145, and 142 °C. Both DNNC and DNNC-d_6 were synthesized, isolated, purified, and characterized in an identical manner and have been reported in detail [14].

2.2. Thermogram curve evaluation

The thermochemical decomposition curves for both DNNC and DNNC-d_6 were evaluated using the $\delta\alpha/\delta t = k\alpha(1-\alpha)$ autocatalytic rate plot equation where (α) is the mole fraction of decomposed DNNC at any given time (t) [2,12,15,16]. To approximate the instantaneous $\delta\alpha/\delta t$ area of curve change, the average change in area (Δa) divided by the time interval distances (Δt) was used ($\Delta a/\Delta t$). Progressive summation of all individual segmented areas along the thermogram curve ($\Sigma\Delta a$) gives the total area under the curve (A), while progressive summation of these areas up to a certain point in time ($\Delta a_0 \ldots \Delta a_n$) gives the amount of decomposed sample (a_n) at that specific time. The mole fraction (α) of decomposed DNNC remaining is given by the fraction of the area under the entire curve up to a certain point ($\alpha = a_n/A$). A graphics plot of $\Delta a/\Delta t$ versus $\alpha(1-\alpha)$ defines an autocatalytic rate behavior where the slope of any linear portion on the curve gives the kinetic rate constant (k).

Previously, individual $\Delta a/\Delta t$ areas have been determined using the curve height above the baseline (h) at given time (t) along the thermogram curve. Because IDSC measures the total heat evolved during the decomposition process, and because this heat evolution is proportional to the global rate at which the sample chemically reacts, the overall rate of decomposition is described by the following approximation: $\delta\alpha/\delta t$ = height (h) divided by the corresponding time along the curve (t). Thus, $\delta\alpha/\delta t = \Delta a/\Delta t = h/t$, or $\delta\alpha/\delta t = h/t$ because h approximates the very small width of the individual $\Delta a/\Delta t$ segment [15].

This height-based approximation has successfully been used for autocatalytic rate plots of IDSC curves where the thermochemical decomposition occurs over a period of minutes [2,11,15–18]. However, these solid state DNNC and DNNC-d_6 thermochemical decomposition processes occurred over many hours (eg. nearly 14 h at 145 °C) [11]. Because the IDSC instrumentation software could plot only a finite number of data points, a long decomposition process possibly gave much larger Δt distance intervals and resultant Δa_n areas. Consequently, the height-based approximation approach, with its very narrow Δt widths and potentially much smaller calculated Δa_n values, was not used. Rather, areas for Δa_n were calculated with measured Δt interval distances using a modification of Simpson's Rule.

Simpson's Rule determines individual areas (Δa_n) at corresponding time distance intervals (Δt_n) located along the baseline of the thermochemical decomposition curve. The standard Simpson's Rule divides a continuous curve into equally distributed time intervals (Δt), and processes these time intervals

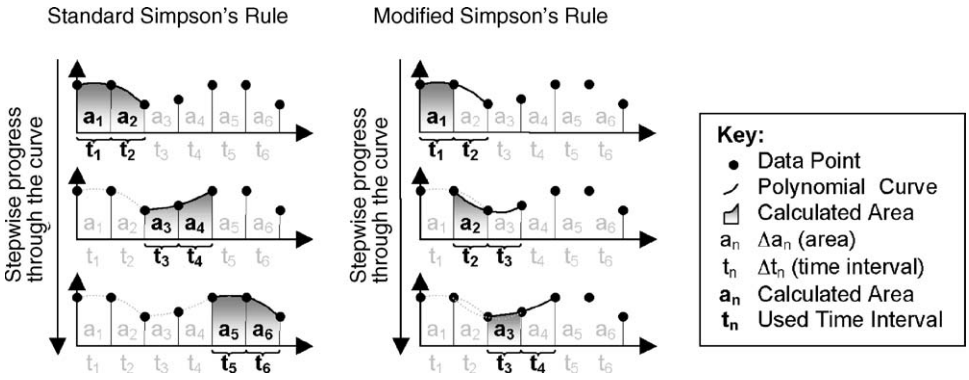

Fig. 2. Standard and modified Simpson's Rules.

in pairs (Δt_n, Δt_{n+1}). Each time interval pair is defined using three data points: (P_1) the start of the first interval, (P_2) the end of the first interval and beginning of the second interval, and (P_3) the end of the second interval. Simpson's Rule uses these three points ($P_{1–3}$) to approximate the polynomial area under the decomposition curve ($\Delta a_n + \Delta a_{n+1}$) for the pair of time intervals ($\Delta t_n + \Delta t_{n+1}$). Using this approach, the area of the entire curve (A), or a large portion of it, may be approximated by aggregating the approximated areas ($\Sigma\Delta a_n$) of each pair of time intervals along the curve.

The standard Simpson's Rule requires the use of pairs of time intervals, which limits the flexibility of the approach because it requires an even number of time intervals to be considered. To rectify this, Simpson's Rule was modified (see Fig. 2) so that, as before, two time intervals are used (Δt_n, Δt_{n+1}) to approximate the original decomposition curve, but unlike before, only the area under the curve of the first interval (Δa_n) is approximated from this curve. To calculate the area for the next interval (Δa_{n+1}), the modified Simpson's Rule approach is reapplied, but with the second and third time intervals (Δt_{n+1}, Δt_{n+2}), respectively. Generally, the modified approach gives us the area under the curve for a single interval (Δa_m) using its and the following corresponding time intervals to generate the curve (Δt_m, Δt_{m+1}). This modified approach allows additional flexibility by making more individual $\Delta a/\Delta t$ sub-intervals available in evaluating linear regression values. Such evaluation permits the optimum limits of linear portions in the autocatalytic rate plot to be determined where a single coherent mechanistic kinetic step produces a kinetic rate constant (k). A software program using a modification of the Simpson's Rule was written and developed to calculate α, Δa, a, and A values for the decomposed DNNC samples.

3. Results and discussion

IDSC measurements taken with maximum instrument sensitivity at 142, 145, and 148 °C reveal that a very slow exothermic solid state DNNC thermochemical decomposition proceeds below its 155–156 °C melting point. Both the endothermic induction period time and exothermic decomposition rate constant data obtained from IDSC curves for DNNC and DNNC-d_6 show a positive kinetic deuterium isotope effect (KDIE). Comparative superimposed decomposition curves taken at 148 °C qualitatively illustrate this positive KDIE where the DNNC decomposition rate proceeds significantly more rapidly than for DNNC-d_6 (Fig. 3). KDIE details identify the rate-controlling step which is a mechanistic feature very important in regulating energetic compound behavior [12,13].

3.1. Physicochemical characteristics

IDSC analyses of DNNC taken at 142, 145, and 148 °C revealed a lengthy 3 (184 min at 148 °C) to nearly 5 h (293 min at 142 °C) endothermic induction period. This induction period was then followed by an exothermic thermochemical decomposition process (Fig. 4) whose autocatalytic rate plot displays three linear segments from which rate constant data could be obtained as illustrated later in Fig. 6. The time required for the solid state decomposition process differs markedly from the liquid state process. For example, liquid state DNNC decomposition at 176 °C is complete in about 42 min (0.7 h) [8,11] while its entire solid state decomposition process at 145 °C requires nearly 14 h or 20-times longer.

Although the thermochemical stability and explosive initiation sensitivity of DNNC more closely resemble that of TNT, the chemical reaction behavior of the solid state DNNC thermochemical decomposition process falls somewhere between its cyclic saturated RDX or HMX nitramine relatives and aromatic TNT.

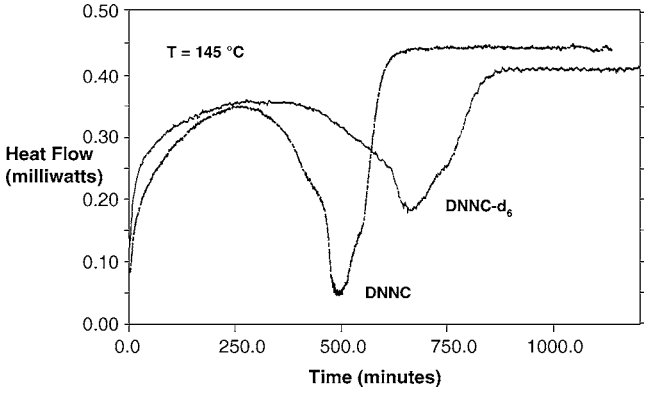

Fig. 3. Real-time IDSC decomposition curve comparison of DNNC and DNNC-d_6 runs at 145 °C.

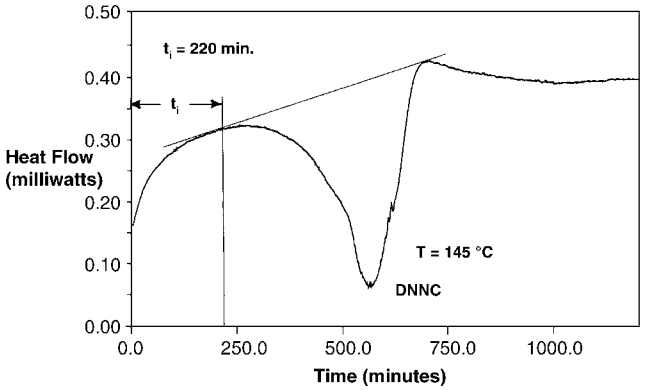

Fig. 4. Induction period (t_i) analysis for a DNNC run at 145 °C.

Over the entire solid state decomposition process, both DNNC and DNNC-d_6 lose an average of 75% sample mass to gaseous product formation and evolution (Table 1). Student *t* statistical analyses of the data in Table 1 confirm that all weight loss values are the same number at a 99.5 confidence correlation. This average weight loss, obtained from 32 sample runs, shows approximately 25% of the original DNNC compound mass remains as condensed phase reaction product(s). In comparison, the HMX nitramine primarily produces only gaseous decomposition products leaving little or no significant condensed phase material after complete decomposition [16] while TNT mainly produces condensed phase decomposition products [17,27–29].

The presence of condensed decomposition products should instill some caution when evaluating KDIE values and assigning the homolytic bond rupture that controls the rate at which a thermochemical decomposition process proceeds. Condensed phase product formation introduces mechanistic consequences which potentially dilute or reduce a true primary KDIE value below its accepted 1.35 experimental minimum. This situation incorrectly can suggest a false secondary KDIE value in the 1.01–1.34 range [12,17].

3.2. Kinetic and mechanistic characteristics

3.2.1. Endothermic induction period curve portion

The endothermic induction period (t_i) seen in Fig. 4 can be evaluated for a kinetic deuterium isotope effect (KDIE) using a ratio of the DNNC-d_6 and DNNC induction times, t_{id}/t_{ih}. This

Table 1
Solid state DNNC and DNNC-d_6 thermochemical decomposition mass losses

Compound	Temperature (°C)	Mass loss (%)	S.D.
DNNC	148	78.5	±5.1
DNNC-d_6	148	74.7	±1.8
DNNC	145	75.5	±3.3
DNNC-d_6	145	71.7	±1.4
DNNC	142	75.2	±1.5
DNNC-d_6	142	72.9	±1.3
Average		74.8	

Table 2
KDIE data for induction period (t_i) portion of the thermochemical decomposition process

Compound	Temperature (°C)	t_i (min)	S.D.	KDIE (t_d/t_h)
DNNC-d_6	148	210	±8	–
DNNC	148	184	±18	1.14
DNNC-d_6	145	316	±31	–
DNNC	145	251	±19	1.26
DNNC-d_6	142	365	±75	–
DNNC	142	293	±67	1.25
Average				1.22

was first demonstrated with the liquid TNT thermochemical decomposition process [17].

Assuming a short temperature equilibration time during the induction period of the solid state DNNC sample, and that other non-kinetic crystal lattice or physicochemical factors are not present that might dilute or mask a true primary KDIE value, the t_{id}/t_{ih} induction period ratio reveals a KDIE equal to 1.22 (Table 2). Because assignment of the induction period termination point for each decomposition curve often is no more accurate than ±10 min, the standard deviations (S.D.) at 148 and 145 °C can be treated as statistically significant. Presupposing that a small concentration of catalytic species forms from DNNC, which then initiates the autocatalytic exothermic solid state decomposition process, this secondary KDIE value would suggest the rate-controlling step occurs either by pendant N–NO_2, pendant C–NO_2, or more likely, ring C–N homolytic bond cleavage. Previous studies with the related RDX nitramine and larger HMX nitramine have addressed both possible N–NO_2 and ring C–N bond cleavage occurring during the decomposition process, but not as the rate-controlling step [24–26,30–37]. The one exception was a rate-controlling homolytic ring C–N bond rupture detected during the decay portion of the solid HMX decomposition process once the HMX entered into a liquid phase [16].

Previously, a primary KDIE of 1.66 was found in the induction period for the liquid state TNT decomposition, and further HPLC investigation revealed a small concentration of catalytic species formed by a rate-controlling step involving pendant methyl group C–H bond rupture from the TNT itself. This rate-controlling homolytic C–H bond rupture required an activation energy equal to 194.6 kJ/mol. Upon reaching a threshold concentration, the catalytic species initiated the TNT exothermic decomposition [17]. Because the endothermic DNNC induction period transitions into an autocatalytic exothermic decomposition, induction period formation of a catalytic species from DNNC also could be possible.

Plotting $\ln t_i$ versus $1/T$ affords a 128.1 kJ/mol activation energy for the DNNC endothermic induction period with a 0.990 linear regression data correlation (Fig. 5). Interestingly, this solid state DNNC induction period activation energy is significantly lower than the analogous induction period activation energies found during the neat thermochemical decomposition process with liquid state DNNC (185.0 kJ/mol) [11] and liquid state TNT (194.6 kJ/mol) [17], where in both

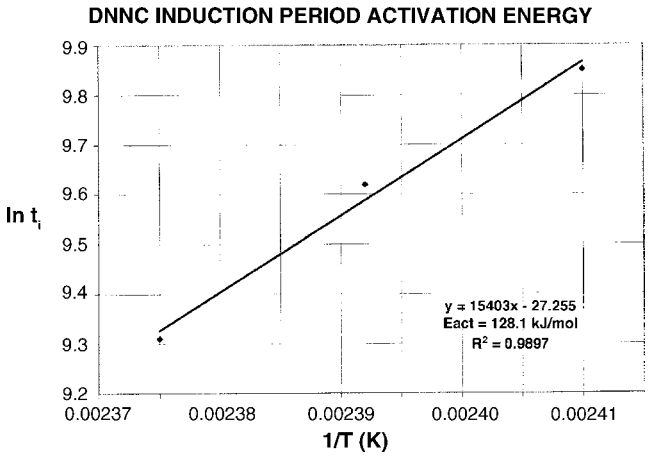

Fig. 5. Energy of activation for induction period of DNNC decomposition curve from 142 to 148 °C.

cases, homolytic C–H bond rupture was the rate-controlling step.

3.2.2. Exothermic early acceleratory curve portion (A)

Following the endothermic induction period, a DNNC exothermic decomposition is initiated that follows an autocatalytic rate behavior. The autocatalytic rate plot reveals three linear segments for the DNNC and DNNC-d_6 at 145 and 148 °C (Fig. 6). These linear segments occur in the early acceleratory portion (A), the later acceleratory portion near the maximum heat release peak (B), and in the decay portion (C) of the decomposition curve. The slope of these three linear portions can provide rate constant (k) data where an exothermic

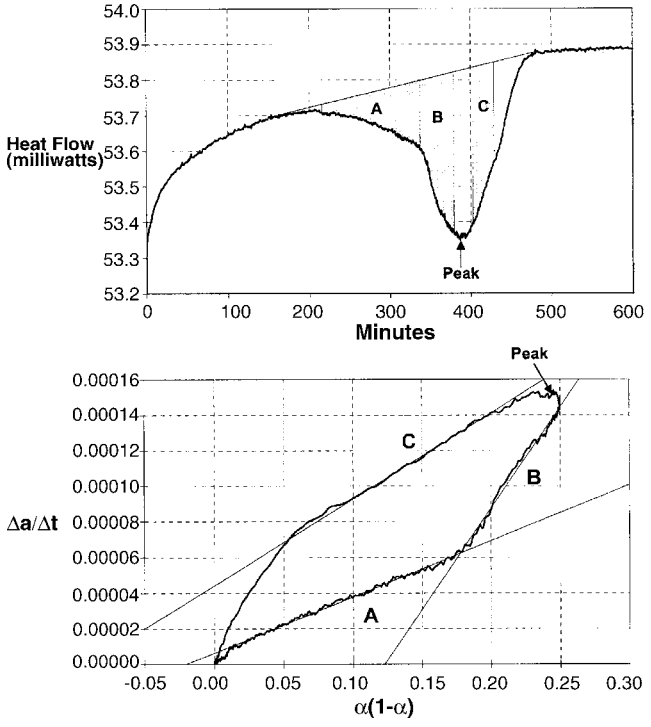

Fig. 6. Comparison of DNNC IDSC decomposition curve (top) obtained at 148 °C and corresponding autocatalytic rate plot (bottom).

Table 3
Height-based vs. increment-based DNNC autocatalytic plot rate constants[a] at 148 °C

Method	Early acceleration (A)	Later acceleration (B)	Decay phase (C)
Height-based	3.25 ± 0.23	9.06 ± 1.71	4.49 ± 0.45
Increment-based	3.28 ± 0.25	8.94 ± 1.73	4.58 ± 0.48

± Data variations represent 1 S.D.
[a] Rate constant values × 10^{-4} s^{-1}.

coherent, steady-state process occurs from one predominating reaction pathway [16]. At the lowest 142 °C temperature, only the early acceleratory (A) and decay portions (C) of the exothermic decomposition curve show linearity. Linearity in the later acceleratory portion (B) disappears and may not be kinetically driven. Combining these two or three linear segment percentages for each curve, the total percent that the thermogram curves follow autocatalytic rate kinetics, within the 142–148 °C temperature spread, is quite high ranging from 62 to 66% for DNNC and 64 to 76% for DNNC-d_6.

The extended 10–14 h duration, covered by the solid state DNNC decomposition process, coupled with limited number of data points the IDSC instrument can store, suggested that more accurate partial $\Delta a/\Delta t$ curve area measurements, than previously used, might be necessary. A more rigorous increment-based autocatalytic rate plot program, described in Section 2, was developed to obtain the reaction rate constants, and derived KDIE values presented in this article.

Several IDSC runs were evaluated using a formerly reported height-based approximation to obtain the $\Delta a/\Delta t$ values comprising the autocatalytic rate plot [15]. Although an approximation, the height-based autocatalytic rate constant values are surprisingly similar to those obtained using the newer increment-based autocatalytic rate program used in this investigation (Table 3) and suggest this approximation is quite reasonable.

Table 4 illustrates the more rigorous increment-based autocatalytic rate constant values obtained at 142, 145, and 148 °C during the early exothermic acceleratory portion (A) of the DNNC and DNNC-d_6 decomposition processes. Particularly noteworthy are the exceptionally high linear regression correlation values for the autocatalytic rate plots.

Table 4
Kinetic data for early acceleratory portion (A) of the thermochemical decomposition process

Compound	Temperature (°C)	$k \times 10^{-4}$ (s^{-1})	S.D. × 10^{-4}	KDIE	R^2
DNNC	148	3.38	±0.24	–	0.998
DNNC-d_6	148	2.51	±0.16	1.35	0.994
DNNC	145	3.13	±0.36	–	0.997
DNNC-d_6	145	2.02	±0.14	1.55	0.995
DNNC	142	2.36	±0.10	–	0.998
DNNC-d_6	142	1.56	±0.26	1.51	0.995
Average				1.47	

R^2 = linear correlation fit to early acceleratory portion of the autocatalytic rate plot.

Table 5
Percentage of IDSC decomposition curve covered by the linear early acceleratory portion (A)

Compound	Temperature (°C)	% Decomposition	S.D.	R^2
DNNC	148	16.7	±7.9	0.998
DNNC-d_6	148	16.2	±5.6	0.994
DNNC	145	18.2	±6.3	0.997
DNNC-d_6	145	26.9	±5.1	0.995
DNNC	142	37.6	±3.1	0.998
DNNC-d_6	142	39.5	±4.9	0.994

R^2 = linear correlation fit to early acceleratory portion of the autocatalytic rate plot.

Table 6
Kinetic data for later acceleratory portion (B) of the thermochemical decomposition process

Compound	Temperature (°C)	"$k \times 10^{-4}$" (s^{-1})	S.D. × 10^{-4}	KDIE	R^2
DNNC	148	8.70	±0.36	–	0.997
DNNC-d_6	148	5.45	±0.95	1.60	0.997
DNNC	145	14.74	±0.47	–	0.994
DNNC-d_6	145	8.74	±0.34	1.69	0.984
Average				1.64	

R^2 = linear correlation fit to latter acceleratory portion of the autocatalytic rate plot.

The early exothermic acceleratory portion (A) provides an average KDIE value equal to 1.47 over the 142–148 °C temperature range and strongly suggests a primary KDIE is present. This 1.47 value comes from linear fits to the autocatalytic rate plot that afford very impressive 0.998 (DNNC) and 0.994 (DNNC-d_6) least squares fitted correlation factors (R^2). This primary 1.47 KDIE value for (A) suggests that homolytic C–H bond rupture, in one type or both types of chemically non-equivalent DNNC methylene groups, constitutes the rate-controlling step. The 1.47 value comfortably exceeds the theoretical high-temperature lower limit of 1.41 and the experimentally accepted 1.35 lower limit for a primary KDIE [12,16–18]. Assignment of a primary KDIE further is supported by a mathematically normalized KDIE value of 2.52 at standard 298 K (25 °C) temperature calculated from the experimental 1.47 KDIE value using an average decomposition temperature of 145 °C [38]. At 25 °C, a 2.5 value constitutes the accepted minimum threshold for a primary KDIE [39]. This linear early acceleratory portion (A) for DNNC constitutes 16–18% of the total decomposition curve at 148 and 145 °C, respectively, but noticeably increases to 38% at 142 °C (Table 5).

The DNNC-d_6 energy of activation was determined for this exothermic early acceleratory portion (A) of the decomposition process. By plotting its respective rate constant logarithm against each corresponding reciprocal temperature (Fig. 7), a

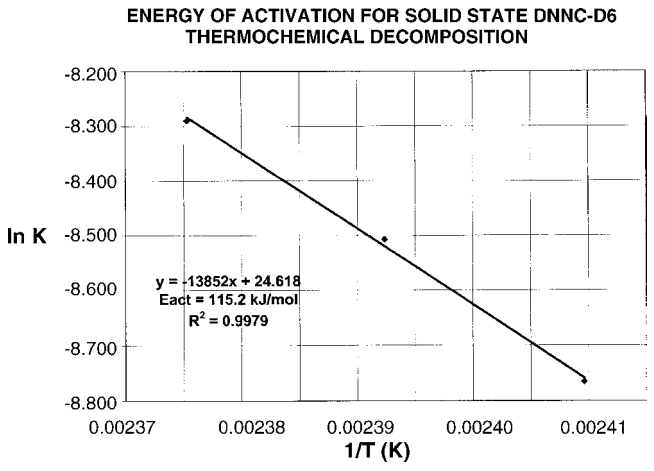

Fig. 7. Energy of activation for early exothermic acceleratory portion (A) of DNNC-d_6 decomposition curve from 142 to 148 °C.

115.2 kJ/mol activation energy for DNNC-d_6 was obtained with an exceptional 0.998 linear regression correlation (R^2). If the rate-controlling methylene C–H bond rupture occurs during the activation step, a lower energy of activation for unlabeled DNNC should result. Because the ground state zero vibrational energy difference between the C–H and the stronger C–D bond is 9.6 kJ/mol (2.3 kcal/mol), the DNNC activation energy then would be expected to be 9.6 kJ/mol less than DNNC-d_6 or around 105.6 kJ/mol. An analogous energy of activation plot of Fig. 6 for DNNC gave an activation energy equal to 87.1 kJ/mol, but with only a lower 0.904 linear regression correlation. Considering this much lower linear regression correlation, the DNNC 105.6 kJ/mol energy of activation data appears to be more reasonable and reliable. This 105.6 kJ/mol activation energy is about 22 kJ/mol lower than the 128.1 kJ/mol activation energy for the DNNC induction period. This point further supports the possibility that a small threshold concentration of catalytic species forms from DNNC during the endothermic induction period to lower the decomposition activation energy and initiate the exothermic acceleratory decomposition. If this is so, the catalytic species forms by a different rate-limiting step than the C–H bond rupture that controls the energy release rate during the entire exothermic decomposition process. With its higher endothermic induction period activation energy, and a lower energy of activation for the exothermic early acceleratory decomposition, DNNC mirrors the same activation energy pattern as TNT where a small amount of TNT converts to a catalytic species that initiates its exothermic decomposition process. Coupled with the autocatalytic nature of the DNNC decomposition process, this same energy of activation pattern further supports the possibility of catalytic species formation during the DNNC induction period.

3.2.3. Exothermic later acceleratory curve portion (B)

The latter acceleratory portion (B) for the solid-state DNNC and DNNC-d_6 decomposition process (Fig. 6) appears to give an average primary KDIE value of 1.64 at 148 and 145 °C. The linear segment of the autocatalytic rate plot covers 22–26% of the total decomposition curve at the 148 °C, decreases to 10–14% at 145 °C, and disappears at 142 °C. This linear segment also reveals a very unusual characteristic indicating the decomposition process at this point is influenced by some factor other than normal kinetics behavior (Table 6).

Table 7
Kinetic data of the decay portion (C) of the thermochemical decomposition process

Compound	Temperature (°C)	$k \times 10^{-4}$ (s^{-1})	S.D. $\times 10^{-4}$	KDIE	R^2
DNNC	148	4.36	±0.52	–	0.996
DNNC-d_6	148	3.52	±0.65	1.24	0.992
DNNC	145	3.13	±0.32	–	0.988
DNNC-d_6	145	2.78	±0.78	1.13	0.973
DNNC	142	2.19	±0.46	–	0.976
DNNC-d_6	142	1.53	±0.36	1.43	0.970
Average				1.27	

R^2 = linear correlation fit to the decay portion of the autocatalytic rate plot.

The "apparent" rate constant, obtained at 148 and 145 °C, increases at the lower temperature with both DNNC and DNNC-d_6. We have no current explanation for this very unusual result, and dismiss this data as being generated by pure kinetic behavior.

3.2.4. Exothermic decay curve portion (C)

The decay portion (C) of the DNNC thermochemical decomposition provides a k_h/k_d KDIE rate constant ratio equal to1.27 (Table 7). This linear segment of the autocatalytic rate plot covers 22–34% of the total decomposition curve for DNNC and a similar 26–34% for DNNC-d_6. By magnitude alone, the 1.27 value could suggest a secondary KDIE since it falls within a 1.01–1.34 experimental range and would be a change in the rate-controlling mechanistic step from the homoyltic C–H bond cleavage observed in the early acceleratory portion (A). This is the case for the HMX nitramine, where the rate-controlling C–H bond rupture defines the rate-controlling solid state decomposition, but then transitions to a rate-controlling ring C–N bond cleavage in its liquified state [16]. Unlike DNNC, however, HMX essentially leaves no significant amount of condensed phase byproduct(s) in the 275–280 °C temperature range when its decomposition process is complete [16]. The presence of 25% condensed phase DNNC decomposition product residue, after completion of the exothermic decomposition process, introduces the possibility that a primary KDIE value for decay portion (C) is being reduced or diluted to the magnitude associated with a secondary KDIE. Reactions that form these condensed phase DNNC decomposition product condensed phase products by a rate-controlling step not involving C–H bond rupture can account for this behavior. Such a dilution of a primary KDIE value has been documented in the decay portion of both the liquid state TNT [12,17] and solid state TATB [2,12,23] decomposition processes. Secondly, even if the DNNC samples transitioned into the liquid state during this decay portion, KDIE thermochemical decomposition studies conducted on liquid DNNC and DNNC-d_6 show no evidence of a secondary KDIE [11,40]. This further suggests the 1.27 KDIE value for the DNNC decay portion (C) of the IDSC thermogram, likely is a diluted primary KDIE value. If so, once initiated, homolytic C–H bond rupture constitutes the rate-controlling throughout the entire exothermic DNNC decomposition process.

3.3. Mechanistic summary

The possible endothermic induction period formation of a catalytic species from DNNC itself, theoretically could result from either a pendant N–NO_2, pendant C–NO_2, but most likely a ring C–N rate-controlling bond rupture suggested by the secondary 1.21 KDIE value. A plethora of past cyclic nitramine decomposition data show that pendant N–NO_2 homolysis, the weakest bond in the nitramine molecule, initiates the decomposition process, followed by a C–N bond rupture which could be rate-controlling. A former DNNC study suggests that either pendant C–NO_2, or possibly N–NO_2 bond rupture (the DNNC molecule's two weakest bonds) is the first step that determines the decomposition reaction pathway which subsequently involves a ring C–N bond cleavage step [3]. Once formed in a threshold concentration, a possible catalytic species then could initiate the solid state DNNC exothermic thermochemical decomposition where the rate controlling step transitions from a possible C–N ring bond rupture to C–H bond rupture. The 1.47 primary KDIE value for the early exothermic acceleratory portion (A) reveals this rate-controlling C–H bond rupture transition which appears to regulate the rest of the exothermic decomposition process.

Past mechanistic IDSC-based KDIE thermochemical decomposition studies of liquid state TNT [17], solid state TATB [2], solid state HMX [16], and liquid state RDX [18] clearly reinforce the mechanistic importance that the early portion of the thermochemical decomposition curve contributes to the overall decomposition process. KDIE values obtained from a thermogram curve, either during an induction period or during the early acceleratory phase, reveal the key mechanistic rate-controlling step that determines the overall decomposition rate. These regions of the IDSC thermgram curve, corresponding to the early portions of the thermochemical decomposition process, are least affected by additional complicating mechanistic factors.

The results of this study support a previous neat DNNC thermochemical decomposition investigation where plausible mechanistic proposals were discussed. The mechanistic proposals were based upon gaseous products generated under bimolecular decomposition conditions representative of a burning surface [3]. Proposed from this gaseous product study was a three-stage process involving three possible and competing DNNC mechanistic decomposition pathways. While many plausible secondary decomposition reactions could occur either from an initial C–NO_2 (5-position) or N–NO_2 (1- and 3-positions) homolytic bond rupture, predominant initiation via C–NO_2 homolysis was selected for mechanistic discussion purposes [3]. An endothermic first stage suggests that NO_2 radical formation, from C–NO_2 homolysis, could be followed by two different subsequent reaction pathways where each contains a homolytic ring C–N bond rupture. The appearance of a secondary KDIE, during the endothermic induction period in our IDSC study of the solid state DNNC decomposition process, is consistent with either of these previously suggested pathways and shows homolytic C–N bond rupture could be the rate-controlling step during this early first stage.

Next in the previous DNNC decomposition study, an exothermic second stage is described which causes a sharp increase in NO and NO_2 gaseous products. This behavior is consistent with the primary KDIE we observed during the early exothermic acceleratory portion (A) of the IDSC thermogram where C–H bond homolysis, possibly at the 2- or 4-positons, becomes the predominating rate-controlling step. Following an initial C–NO_2 or N–NO_2 bond homolysis to produce the NO_2 radical, subsequent NO_2 radical abstraction of a methylene hydrogen atom from the remaining cyclic DNNC ring structure would form HONO [16], an unstable molecule where 2 mol decompose into 1 mol of NO, NO_2, and H_2O gaseous products. A subsequent C–N ring opening, adjacent to the lower energy allylic ring nitrogen at the 1- or 3-positions in the cyclic DNNC fragment, is consistent with a third reaction pathway suggested [3].

Rate-controlling C–H homolysis, occurring late in the decay portion (C) of our decomposition process, also is consistent with the previously discussed third stage where a small amount of HONO was found [3]. Bimolecular recombination reactions would produce the observed condensed phase residue [3] found in the IDSC pans once the solid state thermochemical decomposition process is complete (Table 1). The late third stage appearance of HONO, and nonvolatile condensed phase residue formation by other reactions, possibly not involving a C–H rate-controlling bond rupture, further suggests the 1.27 KDIE value seen in the late decay portion (C) of the IDSC thermogram was a masked or diluted primary KDIE value.

As previously noted, initial N–NO_2 homolysis cannot be ruled out [3]. An NO_2 radical formation from N–NO_2 homolysis, a subsequent rate-controlling hydrogen atom abstraction from the methylene at the 2-position (eg. C–H bond rupture) to form unstable HONO, followed by a subsequent ring opening, like that proposed for HMX, [16] also could explain the second and third stage [3] gaseous products previously reported [3]. Additionally, this alternative pathway would be consistent with the primary KDIE found in this study during the exothermic acceleratory portion of the decomposition process.

4. Conclusions

The early portion the DNNC/DNNC-d_6 thermochemical decomposition process clearly exerts a major role in determining the specific chemical bond rupture that controls the energy release rate of the decomposition process. This point is reflected in previously reported mechanistic KDIE-based IDSC thermochemical decomposition investigations with liquid state TNT/TNT-α-d_3, solid state TATB/TATB-d_6, solid state HMX/HMX-d_8, and liquid state RDX/RDX-d_6.

Within the temperature range investigated, a secondary 1.22 KDIE value for the initial endothermic induction period in DNNC thermochemical decomposition behavior likely indicates a rate-controlling ring C–N bond cleavage could be forming a catalytic species, which upon reaching a small threshold concentration, initiates its subsequent autocatalytic exothermic energy release rate behavior. A lower 105.6 kJ/mol activation energy for the subsequent autocatalytic exothermic decomposition, following a higher induction period 128.1 kJ/mol activation energy, further supports endothermic induction period formation of a catalytic species from DNNC itself. This same mechanistic behavior previously was reported for the liquid TNT decomposition process which followed the same energy of activation pattern. The endothermic induction period results are consistent with a previously suggested mechanistic pathway for the first stage DNNC decomposition process found in a representative burning surface.

Upon initiating the exothermic thermochemical decomposition process, the early acceleratory portion (A) of the DNNC decomposition curve shows a 1.47 KDIE value suggesting that the rate-controlling step transitions to a C–H bond rupture at one or both types of chemically non-equivalent ring methylene groups in DNNC molecule. This rate-controlling C–H bond homolysis likely predominates throughout the remaining exothermic decomposition process. Again, this result supports previously proposed mechanistic pathways for an exothermic second and third stage DNNC surface decomposition process that simulates surface combustion conditions. The DNNC 105.6 kJ/mol activation energy in the early exothermic acceleratory portion (A) for decomposition process can be obtained from a measured 115.2 kJ/mol DNNC-d_6 activation energy.

Acknowledgments

The authors gratefully thank the following individuals: Dr. Kenneth A. Martin, Dr. Victor L. Heasley, and Dr. Dale F. Shellhamer, Department of Chemistry, Pt. Loma Nazarene University, San Diego, CA, for helpful scientific discussions, key software support, and on-site computer assistance in the preparation of this manuscript. Mr. Dean Richards, AF Research Laboratory (AFRL), Edwards AFB, CA, provided critical computer graphics support. Dr. Jerry Boatz (AFRL) and Dr. Karl O. Christe (AFRL) contributed pertinent technical comments and discussion during manuscript preparation. Dr. John Belletire (ERC, Inc. @ AFRL) provided critical review of the written manuscript. The Air Force Office of Scientific Research (AFOSR) is gratefully acknowledged for funding this research study.

References

[1] A.K. Galwey, M.E. Brown, Thermal Decomposition of Ionic Solids, Elsevier, Amsterdam, 1999, Chapter 1, pp. 1–2.
[2] R.N. Rogers, J.L. Janney, M.H. Ebinger, Thermochim. Acta 59 (1982) 287–298.
[3] T.B. Brill, D.G. Patil, J. Duterque, G. Lengelle, Combust. Flame 95 (1993) 183–190.
[4] S.A. Shackelford, B.B. Goshgarian, R.D. Chapman, R.E. Askins, D.A. Flanigan, R.N. Rogers, Propellants, Explos. Pyrotech. 14 (1989) 93–102.
[5] D.L. Levins, C.D. Bedford, C.L. Coon, U.S. Patent 4,346,222 (1982), SRI International, USA.
[6] D.A. Cichra, H.G. Adolph, J. Org. Chem. 47 (1982) 2472–2476.
[7] J. Boileau, M. Piteau, G. Jacob, Propellants, Explos. Pyrotech. 15 (1990) 38. The subject DNNC compound also has appeared in the literature under the acronym of TNDA.
[8] S.A. Shackelford, J.F. Goldman, Propellants, Explos. Pyrotech. 20 (1995) 1–4, and references cited therein.
[9] J. Wang, K.R. Brower, D.L. Naud, J. Org. Chem. 62 (1997) 9055–9060.
[10] B.D. Roos, T.B. Brill, Propellants, Explos. Pyrotech. 28 (2003) 65–71.

[11] S.A. Shackelford, J.F. Goldman, J.A. Menapace, S.A. Hendrickson, 35th International Annual Conference of ICT, Karlsruhe, Germany, June 29–July 2, 2004.
[12] S.A. Shackelford, in: S.N. Bulusu (Ed.), Chemistry and Physics of Energetic Materials, NATO ASI Series, Series C, vol. 309, Kluwer Academic Press, Dordrecht, NL, 1990, Chapter 18, pp. 413–432 & Chapter 19, pp. 433–456.
[13] S.A. Shackelford, J. Phys. IV, Colloque C4, Suppl. to J. Phys. III 5 (1995) 485–499.
[14] S.A. Shackelford, J. Labeled Compds. Radiopharm. XXIX (1991) 1197–1206.
[15] R.N. Rogers, RCEM Rpt. A-04-87, Research Center for Energetic Materials, New Mexico Tech., Socorro, NM 87081, USA, November 4, 1987, pp. 15–65.
[16] S.A. Shackelford, M.B. Coolidge, B.B. Goshgarian, B.A. Loving, R.N. Rogers, J.L. Janney, M.H. Ebinger, J. Phys. Chem. 89 (1985) 3118–3126.
[17] S.A. Shackelford, J.W. Beckmann, J.S. Wilkes, J. Org. Chem. 42 (1977) 4201–4206.
[18] S.L. Rodgers, M.B. Coolidge, W.J. Lauderdale, S.A. Shackelford, Thermochim. Acta 177 (1991) 151–168.
[19] S.N. Bulusu, D.J. Weinstein, J.R. Autera, R.W. Velicky, J. Phys. Chem. 90 (1986) 4121–4126.
[20] S.A. Shackelford, S.L. Rodgers, R.E. Askins, Propellants, Explos. Pyrotech. 16 (1991) 279–286.
[21] S.N. Bulusu, J.R. Autera, J. Energetic Matls. 1 (1983) 133–140.
[22] J. Sharma, W.L. Garrett, F.J. Owens, V.L. Vogel, J. Phys. Chem. 86 (1982) 1657–1661.
[23] J. Sharma, J.C. Hoffsommer, D.J. Glover, C.S. Coffey, F. Santiago, A. Stolovy, S. Yasuda, in: J.R. Asay, R.A. Graham, G.K. Straub (Eds.), Shock Waves in Condensed Matter, Elsevier, 1984, pp. 543–546.
[24] J. Sharma, J.C. Hoffsommer, D.J. Glover, C.S. Coffey, J.W. Forbes, T.P. Liddiard, W.L. Elban, F. Santiago, 8th International Symposiun on Detonation, Albuquerque, NM, July 15–19, 1985, pp. 725–733.
[25] J. Sharma, J.W. Forbes, C.S. Coffey, T.P. Liddiard, J. Phys. Chem. 91 (1987) 5139–5144.
[26] J. Sharma, J.W. Forbes, C.S. Coffey, T.P. Liddiard, in: S.C. Schmidt, N.C. Holmes (Eds.), Shock Waves in Condensed Matter, Elsevier, 1988, pp. 565–568.
[27] L.A. Wiseman, Bristol Research Ret. No. 51, A. C. 2670, Ministry of Supply, Great Britain, 1942.
[28] R.N. Rogers, Anal. Chem. 39 (1967) 730–733.
[29] J.C. Dacons, H.G. Adolph, M.J. Kamlet, J. Phys. Chem. 74 (1970) 3035–3040.
[30] J.D. Cosgrove, A.J. Owen, Comb. Flame 22 (1974) 19–22.
[31] M.A. Schroeder, in: Proceedings of the 16th JANNAF Combustion Meeting, Monterey, CA, CPIA, The Johns Hopkins University, Laurel, MD, CPIA Publ. No. 308, vol. II, 1979, pp. 17–34.
[32] M.D. Pace, A.D. Britt, W.B. Moniz, J. Energetic Matls. 1 (1983) 141–175.
[33] R.A. Fifer, Fundamentals of solid propellant combustion, in: K.K. Kuo, M. Summerfield (Eds.), Progress in Astronautics and Aeronautics, vol. 90, AIAA Inc., 1984, pp. 178–237.
[34] R. Shaw, F.E. Walker, J. Phys. Chem. 81 (1977) 2572–2576.
[35] J. Kimura, N. Kubota, Prop. Explos. 5 (1980) 1–8.
[36] A.D. Britt, M.D. Pace, W.B. Monitz, J. Energetic Matls. 1 (1983) 367–371.
[37] Y. Shu, B.L. Korsounskii, G.M. Nazin, Russ. Chem. Rev. 73 (2004) 293–307.
[38] T.H. Lowery, K.S. Richardson, Mechanism and Theory in Organic Chemistry, second ed., Harper and Row, New York, 1981, pp. 206–207.
[39] G.W. Klump, Reactivity in Organic Chemistry, L. Birladeanu (transl.), Wiley Interscience, New York, 1982, p. 262.
[40] S.A. Shackelford, J.F. Goldman, 203rd Nat. Am. Chem. Soc. Mtg., San Francisco, CA, USA, April 5–10, 1992;
S.A. Shackelford, J.F. Goldman, 22nd International Annual Conference of ICT, Karlsruhe, Germany, July 2–5, 1991.